Magnetic Tunability via Control of Crystallinity and Size in Polycrystalline Iron Oxide Nanoparticles

Minh Dang Nguyen, Liangzi Deng, Jong Moon Lee, Karla M. Resendez, Maggie Fuller, Supawitch Hoijang, Francisco Robles-Hernandez, Ching-Wu Chu, Dmitri Litvinov, Viktor G. Hadjiev, Shoujun Xu, Manh-Huong Phan, and T. Randall Lee*

Iron oxide nanoparticles (IONPs) are widely used for biomedical applications due to their unique magnetic properties and biocompatibility. However, the controlled synthesis of IONPs with tunable particle sizes and crystallite/grain sizes to achieve desired magnetic functionalities across single-domain and multi-domain size ranges remains an important challenge. Here, a facile synthetic method is used to produce iron oxide nanospheres (IONSs) with controllable size and crystallinity for magnetic tunability. First, highly crystalline Fe_3O_4 IONSs (crystallite sizes above 24 nm) having an average diameter of 50 to 400 nm are synthesized with enhanced ferrimagnetic properties. The magnetic properties of these highly crystalline IONSs are comparable to those of their nanocube counterparts, which typically possess superior magnetic properties. Second, the crystallite size can be widely tuned from 37 to 10 nm while maintaining the overall particle diameter, thereby allowing precise manipulation from the ferrimagnetic to the superparamagnetic state. In addition, demonstrations of reaction scale-up and the proposed growth mechanism of the IONSs are presented. This study highlights the pivotal role of crystal size in controlling the magnetic properties of IONSs and offers a viable means to produce IONSs with magnetic properties desirable for wider applications in sensors, electronics, energy, environmental remediation, and biomedicine.

1. Introduction

Iron oxide nanoparticles (IONPs), such as Fe_3O_4 and γ-Fe_2O_3, have been extensively studied due to their great potential in various applications, including environmental uses, sensing technologies, wave-absorbing materials, and, notably, biomedical applications such as biosensing, magnetic hyperthermia, IR-induced phototherapy, magnetic contrast agents, and targeted drug delivery.[1–10] The primary impetus driving the intensive research and discoveries is rooted in a unique combination of their properties, including environmental friendliness, cost-effectiveness, biocompatibility, half-metallicity, and diverse magnetic characteristics.[11,12] To develop high-performance nanosystems based on IONPs for specific applications, the design and fabrication of highly crystalline IONPs with precise control over size, shape, and nanostructures to achieve the desired magnetic properties constitute critical steps.[13–15] Consequently, the development of synthetic methods capable of achieving such control,

M. D. Nguyen, J. M. Lee, S. Hoijang, S. Xu, T. R. Lee
Department of Chemistry and the Texas Center for Superconductivity
University of Houston
Houston, TX 77204-5003, USA
E-mail: trlee@uh.edu

L. Deng, M. Fuller, C.-W. Chu
Department of Physics and the Texas Center for Superconductivity
University of Houston
Houston, TX 77204-5003, USA

K. M. Resendez
Department of Biomedical Engineering and the Texas Center for Superconductivity
University of Houston
Houston, TX 77204-5003, USA

S. Hoijang
Department of Chemistry, Faculty of Science
Chiang Mai University
Chiang Mai 50200, Thailand

F. Robles-Hernandez
College of Engineering Technology
University of Houston
Houston, TX 77204-5003, USA

D. Litvinov
Department of Electrical and Computer Engineering
University of Houston
Houston, TX 77204-5003, USA

V. G. Hadjiev
Department of Mechanical Engineering and the Texas Center for Superconductivity
University of Houston
Houston, TX 77204-5003, USA

M.-H. Phan
Department of Physics
University of South Florida
Tampa, FL 33620, USA

Table 1. Synthesis and magnetic properties of polycrystalline IONSs via solvothermal method using $FeCl_3$ precursors. (adapted from Table 2 of ref. [11] with modifications).

Diameter [nm]	Precursor & Reagents	Solvent	Size control factor	Grain size [nm]	M_S [emu g^{-1}]	H_C [Oe]	Refs.
200, 400, 800	$FeCl_3 \cdot 6H_2O$, NaAc, PEG	EG	Rxn time	UN	81.9, UN, UN	UN	[23]
31, 53, 71, 93, 141, 174	$FeCl_3$, NaOH, PAA	DEG	NaOH stock solution	≈10	UN, 30.9, UN, 56.7, UN, 63.5	SPM	[36]
280	$FeCl_3 \cdot 6H_2O$, Na-acrylate, NaAc	EG	–	5.9, 6.9, 8.3, 13.5	36.2, 38.7, 46.5, 67.2	SPM	[32]
6, 60, 120, 170		EG, DEG	Solvent composition	10	UN	SPM	
20, 90, 165, 300.	$FeCl_3 \cdot 6H_2O$, NaAc, PVP	EG, DEG	Solvent composition	10-20	62.1, 62.1, 62.8, 63.9	8, *20, 28, 16*	[34]
82, 139, 188, 544, 728, 1116	$FeCl_3 \cdot 6H_2O$, NaAc, PAA, H_2O	EG	H_2O	15.4, 20.7, 23.9, 18.6, 17.7, 17.6	*56, 71, 73, 79, 80,* 80.27	*115, 141, 149, 139, 136, 127*	[24]
100, 135, 150, 175, 275	$FeCl_3 \cdot 6H_2O$, NaAc, PVP	EG	Rxn time	17, 17, 15, 12, 11	69, 72, 65, 32, 56	106, 42, 66, 21, 28	[37]
120, 440, 700	$FeCl_3 \cdot 6H_2O$, NaAc, PEG	EG, DEG	Solvent composition, $FeCl_3$	18, 17, 17	78, 84, 87	62, 73, 72	[35]

UN denotes unknown, as the information was not provided in the literature. SPM denotes superparamagnetic, $H_C = M_R = 0$ (at room temperature). Values in italics indicate that the data were estimated from figures provided in the referenced articles. Value of M_S and H_C at 300K. Chemicals: Polyethylene glycol (PEG), poly(acrylic acid) (PAA), polyvinylpyrrolidone (PVP).

while ensuring a monodisperse size distribution and excellent reproducibility, remains an essential and challenging task for both fundamental and applied sciences.

With enormous potential across diverse application fields, IONPs have been synthesized in a variety of sizes and shapes, displaying a wide range of magnetic properties from superparamagnetic (SPM) to ferrimagnetic (FiM) behavior.[11,13,14,16,17] In addition to the challenge of synthesizing IONPs with controlled size and shape, achieving gram-scale production and enhancing the reproducibility of the synthesis have been the focus of many research groups in recent years.[18–20] Among the various structures of IONPs, spherical IONPs have garnered the most attention, due to ease in synthesis and isotropic magnetic properties. Synthesis has produced particles that range in size from 4 nm to even 1 μm.[21–24] Typically, iron oxide nanospheres (IONSs) with a diameter < 25 nm exhibit a single crystal structure and possess SPM properties. Given the notable potential of SPM IONPs in biomedical applications, extensive research efforts have been directed toward advancing the control and reliability of the synthesis to achieve IONPs with desired sizes, compositions, and magnetic properties.[25–31] Therefore, the scope to further enhance the performance or properties of these small-sized IONSs (< 25 nm) depends on the design of the target applications and the strategies employed for functionalization.

On the other hand, larger IONSs (> 25 nm) typically exhibit a polycrystalline structure and display a wider range of magnetic behaviors, including SPM or FiM properties.[24,32,33] The growth of these polycrystalline IONSs usually initiates with the formation of primary crystals, followed by the agglomeration of these primary crystals to form larger particles.[32] Consequently, their magnetic properties are primarily influenced by two structural parameters: the average diameter of the particle and the crystallite size (also referred to as "grain size"). In here, the crystallite size represents the size of the primary crystal. Tuning these struc-

tural parameters provides an avenue to manipulate their magnetic behaviors and explore potential applications, offering an opportunity for further exploration and discovery.

In view of the developed synthesis methods, the solvothermal approach based on ethylene glycol (EG) solvent systems using iron(III) chloride precursors has been shown to be the most useful, providing a facile synthetic technique to control NP size.[11] **Table 1**, adapted from our review paper with modifications, summarizes the key results in the synthesis of IONSs using the EG solvent system-based method. IONSs synthesized via this method have been reported to exhibit either FiM or SPM properties.[11] Deng et al. were the first to report this method using $FeCl_3 \cdot 6H_2O$ precursors to synthesize Fe_3O_4 NPs with sizes of 200, 400, and 800 nm by controlling the reaction time.[23] Other research groups have explored the use of a binary solvent system comprising EG and diethylene glycol (DEG) to control particle size.[32,34,35] Leung's group also investigated the effects of sodium acetate (NaAc) and sodium acrylate (Na-acrylate) on the size and crystallite size of IONSs.[32] A study by Tong's group emphasized the significant influence of water on both the particle size and crystallite size of IONSs.[24] Despite these efforts, a precise control over the crystallinity of these nanoparticles was not achieved. In this context, we anticipate that large polycrystalline IONSs with enhanced crystallinity may exhibit stronger FiM properties.

It has been shown that FiM IONSs with larger sizes yield higher saturation magnetization (M_S).[24,35] However, the effects of size on the other magnetic parameters, such as coercivity (H_C), as listed in Table 1, are not well documented. On the other hand, crystallinity has been reported to enhance the magnetic properties of IONPs, both M_S and H_C.[11,37] In the case of large-sized IONSs exhibiting SPM properties, with sizes around 280 nm, an increase in grain size (crystallite size) from 5.9 to 13.5 nm, while maintaining the average size, leads to a monotonic increase in M_S from 36.2 to 67.2 emu g^{-1}.[32] Recent reports have highlighted
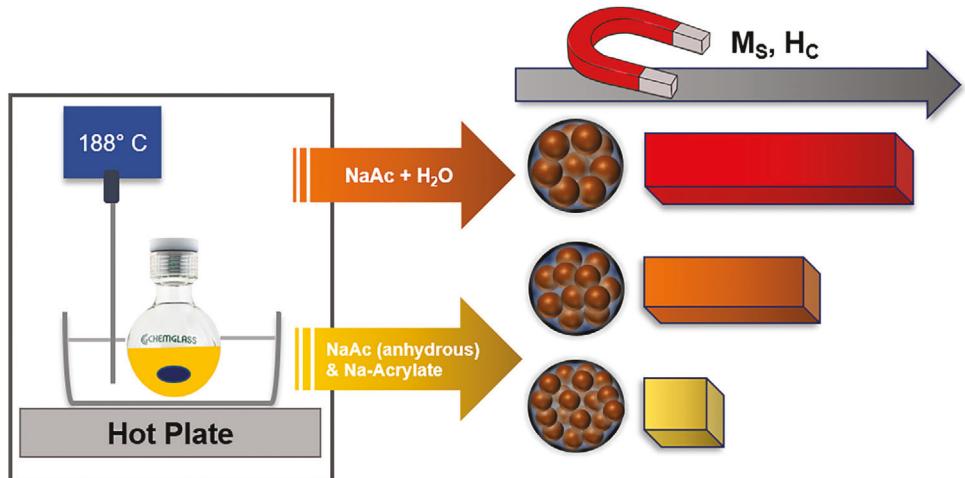
Scheme 1. A modified solvothermal synthesis using different additives to control the crystallinity and magnetic properties of iron oxide nanoparticles.

the superior magnetic properties of Fe_3O_4 nanocubes compared to their nanosphere counterparts.[37–39] Besides factors related to magnetic anisotropy, crystallinity has been identified as the main determinant of the superior magnetic properties of Fe_3O_4 nanocubes.[37] Another notable study by Brougham's group, who examined two iron oxide suspensions consisting of NPs with identical size and cubic shapes, and similar dispersion quality, demonstrated significantly enhanced performance in magnetic hyperthermia and magnetic resonance imaging contrast in samples with better crystallinity and no defects.[40] These findings underscore the critical role of improving the crystallinity of IONSs as a key approach to enhancing their magnetic properties and maximizing their potential in various applications.

Therefore, we envision that the crystallinity (crystallite/grain size) of the IONSs is the key parameter for manipulating their magnetic properties and customizing the nanoparticles for a wide range of applications. To provide a deeper understanding of the structure-to-properties relationships and to enhance the application potential of IONSs, it is crucial to develop a more refined synthetic approach with comprehensive capabilities, including: 1) producing IONSs with highly uniform size and spherical shape, 2) precisely controlling particle structure, including both size and crystallinity, 3) widely and finely tuning the magnetic properties of nanoparticles from ferrimagnetic (FiM) to superparamagnetic (SPM), and 4) achieving simplicity in technical aspects that are needed for scaling-up the reaction. To date, no synthetic approach has satisfied all these criteria to become a versatile method for preparing IONPs.

The overall aim of our research is to address the challenges mentioned above by advancing the well-established solvothermal method through controlling additives used, as illustrated in **Scheme 1**. We present here an efficient synthetic approach to produce highly crystalline IONSs with crystal sizes exceeding 24 nm across a broad range of size (50 to 400 nm) and to control the crystallinity of IONSs over a wide range (from 37 to 10 nm). Using $NaAc \cdot 3H_2O$ combined with varying binary solvent systems, stirring speeds, and ramping rates, we successfully synthesized Fe_3O_4 nanospheres with sizes from 52 to 393 nm, all of which exhibit highly crystalline structures and uniform morphologies.

The magnetic properties of these highly crystalline IONSs are comparable to those of the single-crystalline Fe_3O_4 nanocubes of similar sizes. We found that while the use of sodium acetate trihydrate was instrumental in enhancing the crystallinity of the IONSs, the use of anhydrous NaAc and sodium acrylate (Na-acrylate) reduced the crystallinity. This, in turn, facilitates fine control of crystallite size over a wide range, offering a valuable means of tuning magnetic properties from the FiM to SPM state without changing particle size. This has been documented by a comprehensive study of the effects of size and crystallinity on the magnetic properties of IONSs. These important findings lead us to propose the growth mechanism of IONSs to achieve adjustable particle sizes and crystallite sizes. This work introduces an efficient synthetic approach with the capacity to fabricate IONSs of the desired size and magnetic properties, thereby serving as an indispensable tool in the design of IONP systems for applications in electronic devices, sensing technologies, and biomedicine.

2. Results and Discussion

2.1. Structural and Magnetic Characterization of Highly Crystalline Iron Oxide Nanospheres

In the context of this paper, the term size refers to the "average diameter" for spherical NPs and the "average edge length" for cubic NPs. The term "crystallite size" is abbreviated as "cs", denoting the average crystallite size, also known as the "grain size" of polycrystalline NPs. By utilizing different binary solvent systems and controlling empirical parameters such as stirring and ramping rates, highly crystalline IONSs with various sizes, from 52 to 393 nm, were successfully synthesized. **Figure 1** displays the SEM images of highly crystalline IONSs with uniform round shapes and narrow size distributions. Larger IONSs appeared to exhibit greater sphericity in their shape. In this method, vigorous stirring (at least 540 rpm) was employed, positively impacting the control of size and shape homogeneity. The slow stirring speed resulted in an extremely polydisperse size distribution of NPs, as illustrated in Figure S1 (Supporting Information).

**ADVANCED
SCIENCE NEWS**

www.advancedsciencenews.com

**NANO · MICRO
small**

www.small-journal.com
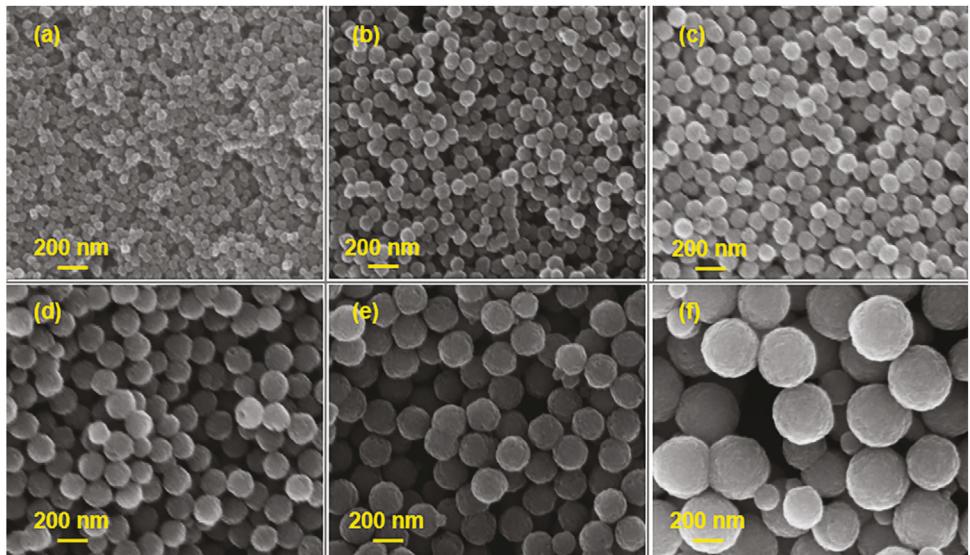
Figure 1. SEM images at 100kX magnification of highly crystalline Fe$_3$O$_4$ nanospheres with average diameters: a) 52 ± 3, b) 98 ± 8, c) 120 ± 9, d) 175 ± 13, e) 220 ± 10, f) 393 ± 27 nm.

Powder X-ray Diffractometry (XRD) was used for phase indexing and to deduce the crystallite size of the NPs. **Figure 2** presents the X-ray diffraction patterns of highly crystalline IONSs, where strong signals with sharp peaks and high intensity indicate highly crystalline structures. The XRD patterns were matched with the JCPDS 01-088-0315 file. In all samples, clear diffraction peaks were observed at 18.35°, 30.18°, 35.55°, 37.19°, 43.21°, 53.61°, 57.15°, and 62.76°, corresponding to the lattice planes (111), (220), (311), (222), (400), (422), (511), and (440), respectively. The calculated values of the crystallite size were 30, 37, 26, and 24 nm for IONSs with average sizes of 52 ± 3, 120 ± 9, 220 ± 10, and 393 ± 27 nm, respectively. All samples exhibited a highly crys-

talline structure with crystallite size ≥ 24 nm. Notably, the sample synthesized from a 15/25 mL EG/DEG (mL) ratio displayed the most crystalline structure. And the crystallinity reduced when more EG was used. In addition, low-intensity peaks at diffraction angles of 71.21°, 74.26°, 75.26°, and 79.24°, clearly visible in the sample synthesized from a 15/25 mL EG/DEG ratio were indexed for (620), (533), (622), and (444), respectively. This further confirmed the highest level of crystallinity in this sample. Despite the well-known effects of solvent mixtures on size control, no observed effects of solvent compositions on the crystallite size were noted. Our experimental results provide evidence that solvent compositions affect the crystallinity of the sample, and a 15/25 mL EG/DEG ratio is the optimal binary solvent ratio for forming a highly crystalline structure. Compared with other reported work (see Table 1), the IONPs presented in Figure 1 not only exhibit highly crystalline structures with unprecedentedly large crystallite sizes (ranging from 24 to 37 nm), but also display highly uniform spherical morphologies and narrow size distributions.

The use of sodium acetate trihydrate, instead of its anhydrous version, resulted in a surprising outcome regarding the level of crystallinity. Liu et al. were the first to report the effects of water on the size and crystallite size of IONSs in solvothermal synthesis.[24] By introducing varying amounts of water into the EG solvent, the size of NPs was controlled from 80 nm to 1 μm with reported crystallite sizes ranging from 15.4 to 23.9 nm. Therefore, we hypothesized that the water content in NaAc·3H$_2$O fell within the optimal range for forming larger primary crystals. To confirm this hypothesis and investigate the effects of water on NP structure, controlled experiments with the addition of water to the synthesis were conducted, and the results are presented in Table S1 (Supporting Information). First, by replacing NaAc·3H$_2$O with anhydrous NaAc while keeping other parameters unchanged, the size of IONSs increased, but all samples had much smaller crystallite sizes (< 20 nm). A series of experiments with a controlled amount of water added to the synthesis were
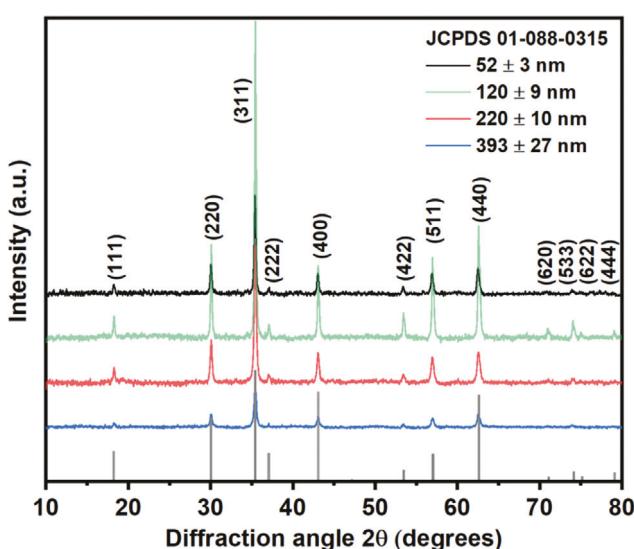

Figure 2. XRD patterns of highly crystalline IONSs with average sizes of 52, 120, 220, and 393 nm synthesized from EG/DEG (mL) mixtures: 10/30, 15/25, 20/20, and 30/10.
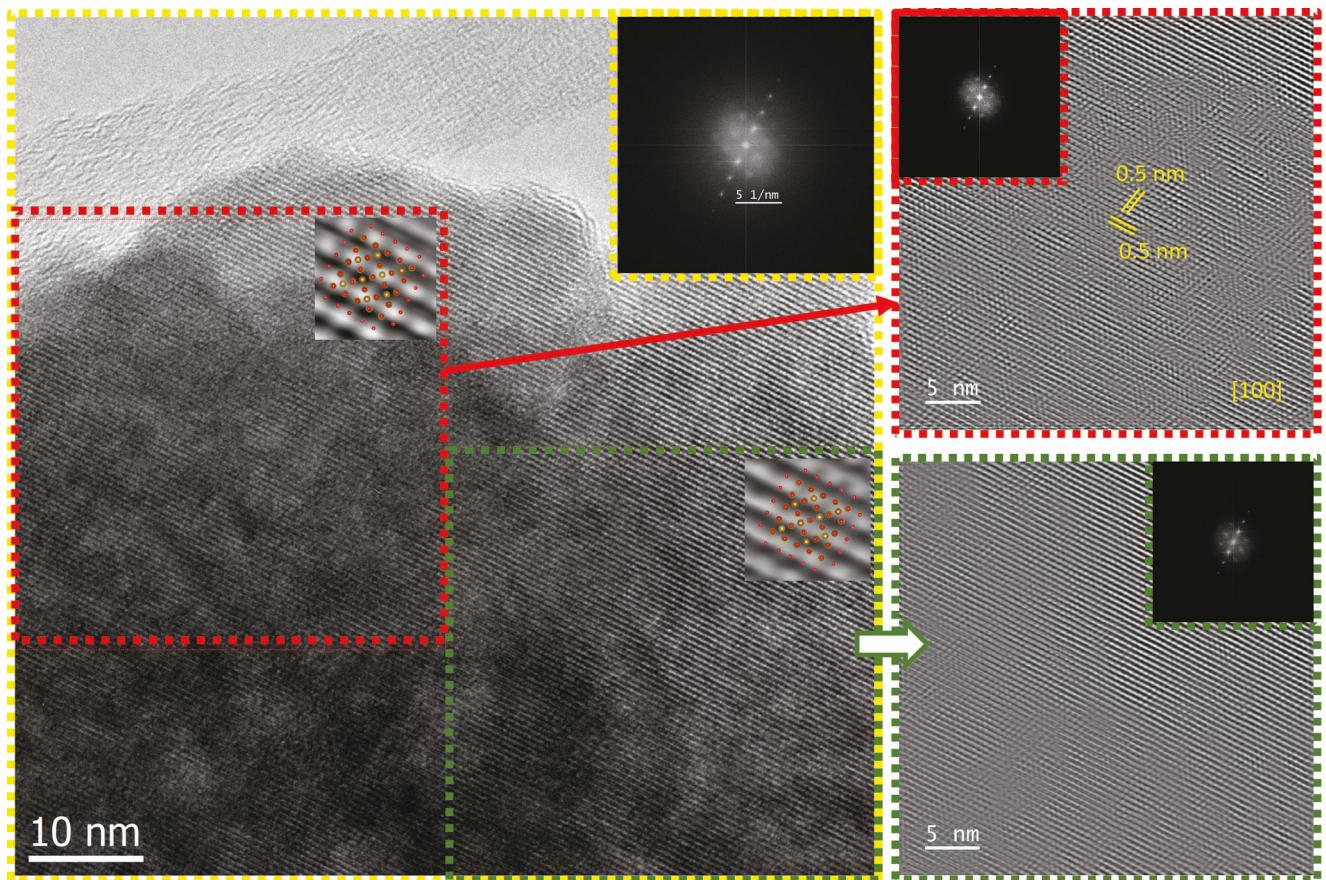
Figure 3. High-resolution TEM image and SAED of IONSs (avg. size 120 ± 9 nm, cs 37 nm).

conducted. Instead of using trihydrate chemicals, using anhydrous chemicals with 2.17 g NaAc and adding a similar amount of water to what is contained in trihydrate chemicals (1.43 mL H_2O), the size and crystallite size showed almost no noticeable change. However, using less water caused an increase in the average size and a decrease in crystallite size. Further investigations by adding more water while still using NaAc·$3H_2O$ were conducted. The addition of a small amount of water, such as 180 µL, caused almost no significant changes in size and crystallite size for both solvent ratios (20/20 and 15/25). However, a larger amount of 540 µL induced noticeable changes in size and crystallinity. While adding more water consistently led to a decrease in size, the crystallite size usually increased up to a certain level before decreasing. It can be said that using a larger amount of water reduces the size, but the effect on crystallite size is not consistently monotonic. There exists a certain range of water amounts that is optimal for producing large primary crystals (crystallite size). These observations are consistent with a previous study by Tong's group, where different amounts of water were added to the synthesis using only EG solvent.[24]

To visualize the highly crystalline structure, a sample of IONSs with the largest crystallite size was characterized by Selected Area Electron Diffraction (SAED) in high-resolution TEM. Simulated Fast Fourier Transform (FFT) diffraction patterns were produced using DigitalMicrograph software from the locations indicated by the insets. **Figure 3** provides an overview of a single crystal

domain where all observable planes have a d-spacing of 0.5 nm, characteristic of the (100) plane. The difference between the theoretical ($d_{(100)}$ = 0.485 nm) and the experimental spacing is ≈3%, which falls within the range of systematic error. The red and green insets show the exact same plane orientation, which is easily identified by observing the three diffraction patterns having the same crystal orientation. The diffraction patterns, along with XRD patterns, collectively confirmed the highly crystalline nature of the NPs.

X-ray photoelectron spectroscopy (XPS) and Raman spectroscopy were used to confirm the phase compositions of iron oxide samples. In **Figure 4a**, the full survey spectra of highly crystalline IONSs display peaks corresponding to Fe 2p, O 1s, C 1s, and Fe 3p. The high-resolution Fe 2p spectra exhibit peaks at 710.4 and 724.1 eV, assigned to Fe $2p_{3/2}$ and Fe $2p_{1/2}$, respectively.[41,42] The broadened features of these two peaks indicated the coexistence of Fe^{2+} and Fe^{3+}. A satellite peak ≈718 eV is commonly observed for the γ-Fe_2O_3 phase, which was absent in the XPS spectrum (Figure 4a), confirming the synthesized Fe_3O_4 NPs. In addition, color of iron oxides can be used to quickly differentiate the phase purity, Figure S2 (Supporting Information) illustrates the color of various Fe^{3+} oxides.[43] Highly crystalline IONSs appear entirely black, indicating the dominant presence of the magnetite (Fe_3O_4) phase, as shown in Figure 4a. The Raman spectrum (Figure 4b), provides further confirmation of the pure magnetite phase, with

ADVANCED
SCIENCE NEWS
www.advancedsciencenews.com

NANO · MICRO
small
www.small-journal.com
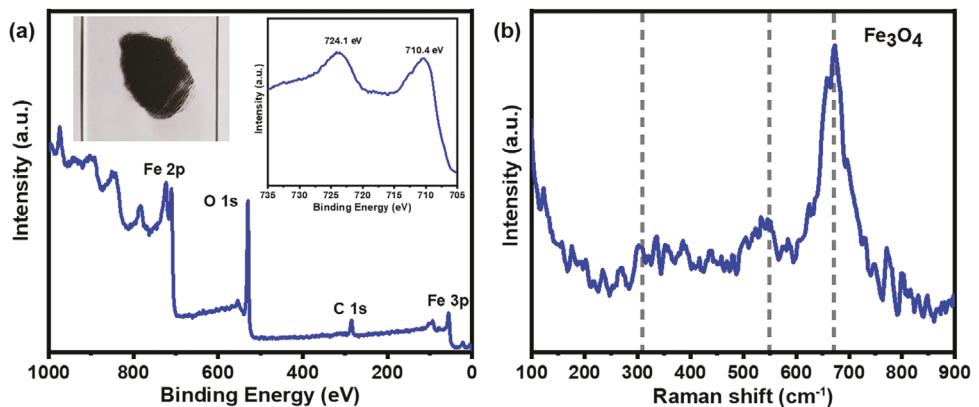
Figure 4. a) XPS spectrum with an optical image of nanoparticle powder and b) Raman spectrum of highly crystalline IONSs.

a major sharp peak at ∼670 cm^{-1} and minor peaks at ∼550 and ∼310 cm^{-1}.[44–46]

The room-temperature magnetic properties of the synthesized IONSs were characterized using a Vibrating Sample Magnetometer (VSM). **Table 2** summarizes the average size, crystallite size, and magnetic parameters (M_S, H_C, and M_r) of these IONSs. It can be seen in this table that all the IONSs exhibit FiM behavior (non-zero values of H_C and M_r) at room temperature. The first observed trend is that an increase in crystallite size leads to higher H_C and M_r values. Samples with crystallite sizes of 24 (particle size 393 nm), 26 (particle size 220 nm), 30 (particle size 52 nm), and 37 nm (particle sizes 98 and 120 nm) exhibited increases in H_C (from 16 to 68 Oe) and M_r (from 3 to 20 emu g^{-1}). For samples with a similar crystalline size (37 nm) but different particle sizes (98 nm vs 120 nm), the larger particles were found to possess slightly stronger FiM properties. It is worth noting that high values of M_S (≈70 emu g^{-1}) are preserved in FiM polycrystalline IONSs with particle sizes varying over a wide range of ≈50 to 400 nm, which are desirable for a variety of biomedical and other applications.

2.2. Highly Crystalline Nanospheres Versus Nanocubes: A Comparative Magnetic Study

In the realm of IONP-based biomedical applications, numerous studies have been conducted to compare the magnetic properties of spherical versus cubic IONPs.[37–39] It has been shown that cubic IONPs exhibit superior magnetic properties compared to their spherical counterparts.[37,47] In our previous study, a comparative analysis of magnetic properties between these two systems revealed that the Fe_3O_4 nanocubes exhibited significantly higher values of M_S (1.4–3.0 times) and H_C (1.1–8.0 times) compared to the Fe_3O_4 nanospheres.[37] To highlight the enhanced magnetism of the above-synthesized polycrystalline IONSs due to their enhanced crystalline structures and their potential applications, we have compared their FiM properties with those of single-crystalline Fe_3O_4 nanocubes of similar sizes synthesized by us using the thermal decomposition method.[16,37,48]

Figure 5 displays TEM images of Fe_3O_4 nanocubes with edge sizes varying from 43 ± 3 nm to 184 ± 23 nm. These iron oxide nanocubes were then compared with the highly crystalline IONSs of the same volume or the same body-diagonal versus diameter to match previous work.[37] The body-diagonal and volume of the synthesized Fe_3O_4 nanocubes, along with the estimates of the equivalent-volume nanospheres, were computed and are presented in **Table 3**. The FiM Fe_3O_4 nanocubes with an average size of 23 ± 4 nm were synthesized to fulfill the comprehensiveness of the study, and a corresponding TEM image is provided in Figure S3 (Supporting Information).

The iron oxide nanocubes were characterized using high-resolution XPS spectra in the Fe 2p region, revealing peaks at 723.9 and 710.8 eV, corresponding to the spin-orbit split double peaks of Fe 2p$_{1/2}$ and Fe 2p$_{3/2}$ of Fe_3O_4. Notably, no satellite features were observed in the 718 eV region, as shown in Figure S4 (Supporting Information), excluding the presence of γ-Fe_2O_3 phase.[41,42] Figure S5 (Supporting Information) shows a single crystal and its respective zoom-out view, along with SAED and HRTEM image. The high-resolution image of the nanocubes exhibits clear lattice fringes along the diagonal of cubic surface, featuring a d-spacing $d_{(220)}$ = 0.29 nm, which matches the value of $d_{(220)}$ = 0.29 nm in JCPDS 01-088-0315 file. It is also important to mention that the particle is a single crystal.

The effects of size on the magnetic properties of Fe_3O_4 nanocubes are clearly delineated from the magnetic data summarized in Table 3. The variation in coercivity follows the transition from the single-domain and multi-domain regime, as illustrated in Figure S6 (Supporting Information).[49] The H_C increases with size until reaching a critical size, above which the

Table 2. Room temperature magnetic properties of polycrystalline Fe_3O_4 nanospheres with large crystallite size.

Average size[a] [nm]	Crystallite size [nm]	M_S [emu g^{-1}]	H_C [Oe]	M_r [emu g^{-1}]
52 ± 3	30	75	59	15
98 ± 8	37	74	64	19
120 ± 9	37	75	68	20
175 ± 13	34	79	77	10
220 ± 10	26	73	41	5
393 ± 27	24	67	16	3

[a] Size means diameter dimension.
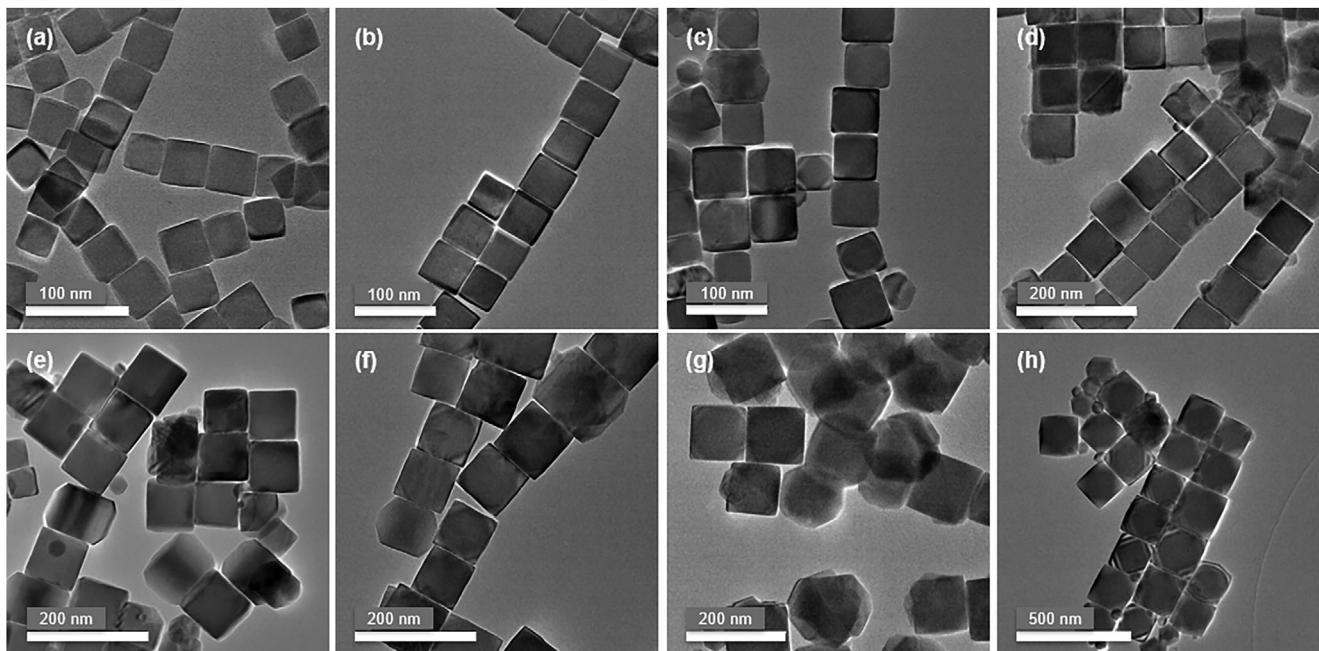
Figure 5. TEM images of Fe_3O_4 nanocubes with various sizes (edge length): a) 43 ± 3, b) 51 ± 3, c) 58 ± 4, d) 69 ± 5, e) 82 ± 5, f) 101 ± 17, g) 119 ± 15, and h) 184 ± 23 nm.

multi-domain state appears to occur, leading to a decrease in coercivity. For the presently synthesized Fe_3O_4 nanocubes, H_C increased from 43 to 138 Oe in the size range of 23 to 82 nm, and then decreased for larger sizes. An edge length of 82 nm (corresponding to the 142-nm body-diagonal dimension) represents approximately the critical size for the Fe_3O_4 nanocubes at which a transition from the single-domain to multi-domain state occurs. It is worth noting that, while the plot illustrated in Figure S6 (Supporting Information) is commonly used to predict the relationship between the particle size and H_C of a magnetic nanoparticle system, it can be adapted to describe the relationship between crystallite size and H_C in the polycrystalline IONSs. Regarding M_S values, it can be concluded that larger nanocubes tend to yield slightly higher M_S values. Table 3 reveals a gradual increase in M_S from 74 emu g^{-1} (size 23 nm) to $\approx$79 to 82 emu g^{-1} (in the size range of 40 to 100 nm), reaching 84 emu g^{-1} for larger nanocubes

(size ≥ 120 nm). Smaller nanocubes, with their higher surface-to-volume ratio, are often known to exhibit a greater proportion of disordered/canted surface spins. Therefore, the presence of disordered/canted surface spins could result in lower M_S values in smaller nanocubes, a phenomenon commonly observed in fine magnetic nanosystems.[11,50,51] By analyzing the size-dependent magnetic properties of the Fe_3O_4 nanocubes, we demonstrate that the relationship established (presented in Figure S6, Supporting Information) for the H_C versus particle size dependence is generally valid for NP systems of single crystalline nature. For the polycrystalline IONSs, however, we have shown that H_C does not scale with particle size but with crystallite size (see Table 2). In the next part, we will discuss in detail the relation between H_C and crystallite size in the polycrystalline IONS system.

Now, we compare the magnetic parameters (M_S, H_C, and M_r) of the Fe_3O_4 nanocubes to those of the Fe_3O_4 nanospheres based

Table 3. Magnetic properties of Fe_3O_4 cubic NPs with various sizes.

Average Size[a] [nm]	Body-Diagonal [nm]	Volume [nm³]	Equivalent-volume Nanospheres [nm]	M_S [emu g^{-1}]	H_C [Oe]	M_r [emu g^{-1}]
23 ± 4	40 ± 7	12167	29	74	43	14
43 ± 3	74 ± 5	79507	53	81	76	23
51 ± 3	88 ± 5	132651	63	80	86	22
58 ± 4	100 ± 7	195112	72	80	87	20
69 ± 5	120 ± 9	328509	86	82	122	24
82 ± 5	142 ± 9	551368	102	81	138	25
101 ± 17	175 ± 29	1030301	125	79	135	21
119 ± 15	206 ± 26	168 5159	148	84	87	19
184 ± 23	319 ± 40	6 229 504	228	84	83	17

[a] Size means edge length dimension.

ADVANCED
SCIENCE NEWS
www.advancedsciencenews.com

NANO · MICRO
small
www.small-journal.com

Table 4. Magnetic properties of Fe_3O_4 cubic and spherical NPs having comparable volumes.

Shape	Edge/diameter [nm]	$\frac{M_S (cube)}{M_S (sphere)}$	$\frac{H_C (cube)}{H_C (sphere)}$	$\frac{M_r (cube)}{M_r (sphere)}$
Cubic Sphere	43 ± 3 52 ± 3	1.08	1.29	1.53
Cubic Sphere	69 ± 5 89 ± 8	1.06	2.03	1.26
Cubic Sphere	82 ± 5 98 ± 8	1.09	2.16	1.32
Cubic Sphere	101 ± 17 120 ± 9	1.06	1.99	1.05
Cubic Sphere	119 ± 15 140 ± 10	1.12	1.74	1.72
Cubic Sphere	184 ± 23 220 ± 10	1.15	2.02	3.40

on the same volume or the same body-diagonal(BD)/diameter.[37] The body-diagonal of the nanocubes was chosen for this comparison because it represents the largest dimension of a cubic shape. Calculated values of BD (BD = edge length * $\sqrt{3}$) and volume (volume = (edge length)^3) of the Fe_3O_4 nanocubes are provided in Table 3. The nanocubes with sizes of 43, 69, 82, 101, 119, and 184 nm are estimated to have volumes equivalent to the nanospheres with sizes of 53, 86, 102, 125, 148, and 228 nm, respectively. Therefore, comparisons of similar volumes are made for the polycrystalline IONSs with average sizes of 52 ± 3, 89 ± 8, 98 ± 8, 120 ± 9, 140 ± 10, and 220 ± 10 nm. **Tables 4** and **5** present the comparative studies of the magnetic parameters of these two systems (nanocubes and nanospheres).

It can be seen from Table 4 and Table 5 that the values of M_S, H_C, and M_r for the Fe_3O_4 nanocubes are 1.0 to 1.15 times, 1.29 to 2.76 times, and 1.05 to 3.4 times higher than those of the Fe_3O_4 IONSs, respectively. Noticeably, the values of M_S are comparable for both systems, which once again indicates that the high crystallinity in the polycrystalline IONSs is crucial in preserving the large M_S values, suggesting that the polycrystalline IONSs

Table 5. Magnetic properties of Fe_3O_4 cubic and spherical NPs having similar body-diagonals/diameters.

Shape	Body-diagonal/diameter [nm]	$\frac{M_S (cube)}{M_S (sphere)}$	$\frac{H_C (cube)}{H_C (sphere)}$	$\frac{M_r (cube)}{M_r (sphere)}$
Cubic Spheres	88 ± 5 89 ± 8	1.04	1.43	1.16
Cubic Spheres	100 ± 7 98 ± 8	1.08	1.36	1.05
Cubic Spheres	120 ± 9 120 ± 9	1.09	1.79	1.20
Cubic Spheres	142 ± 9 140 ± 10	1.08	2.76	2.27
Cubic Spheres	175 ± 29 175 ± 13	1.00	1.75	2.10
Cubic Spheres	206 ± 26 220 ± 10	1.15	2.12	3.08

are very promising for a wide range of biomedical applications. More prominent differences in H_C and M_r are observed in the Fe_3O_4 nanocubes compared to the Fe_3O_4 IONSs, which arise mainly from the greater contribution of both magnetocrystalline and shape anisotropies in the former.[11,51]

2.3. Magnetic Tunability from Ferrimagnetism to Superparamagnetism in Iron Oxide Nanospheres: The Importance of Controlling Crystalline Sizes

As shown above, the crystallite size of the polycrystalline IONSs plays a crucial role in determining their magnetic properties. Therefore, the ability to control crystallinity without altering the average size is crucial for fine-tuning the magnetic properties. Leung's group reported the use of sodium acrylate to adjust the crystallite size from 13.5 to 5.9 nm while maintaining an average particle size of ≈280 nm.[32] However, the magnetic properties of the IONPs were only limited to the SPM regime. It would, therefore, be important to investigate how the magnetic properties of polycrystalline IONPs vary from the FiM to SPM state when crystalline size can be tuned around a critical size. In this context, the critical size means the specific size of primary crystals (crystallite sizes) in the polycrystalline IONSs at which the transition from FiM to SPM properties occurs.

Our synthesis method has enabled us to synthesize IONSs with different crystallite sizes (10 to 37 nm) while keeping the average particle size at ≈160 nm. **Figure 6**, for example, displays the SEM images of IONSs with a similar average size of ≈160 nm but with varying crystallite sizes, ranging from 37, 26, 19, and 12, to 10 nm. Notably, despite the wide variation in crystallite size, the uniform morphology of the nanoparticles is largely maintained. Here, samples with crystallite sizes of 37 and 26 nm, indicating a highly crystalline structure (cs $\geq$ 24 nm), were synthesized using NaAc·$3H_2O$ from a solvent system containing ratios of 15/25 and 20/20 EG/DEG, respectively. By replicating the synthesis of IONSs size 160 ± 10 nm (with a cs of 26 nm), an additional amount of sodium acrylate such as 100 and 200 mg was introduced to reduce the cs to 19 and 10 nm, respectively. While the use of sodium acrylate was efficient in reducing the crystallite size, as previously reported,[32] we observed a broader size distribution and moderate deformation of the round shape. The magnetic properties of these samples were measured using the VSM. **Table 6** summarizes the size, crystallite size, and magnetic properties of these IONSs. It is very interesting to note in this table that the IONSs undergo a transition from the FiM ($H_C \neq 0$, $M_r \neq 0$) to SPM ($H_C = 0$, $M_r = 0$) state, when crystalline size is reduced from 37 to 10 nm. For samples with crystallite sizes of 19, 26, and 37 nm, the FiM properties are achieved, with values of M_S, H_C, and M_r increasing with crystallite size. However, samples with crystallite sizes of 10 and 12 nm, displaying no magnetic hysteresis ($H_c = 0$, $M_r = 0$), exhibit a SPM-like behavior, and their M_S values are 56 and 63 emu g^{-1}, respectively. The increase in M_S values with larger crystallite sizes in these SPM IONSs is consistent with the observations of Leung's group.[32] The critical size of the crystallite size in polycrystalline IONSs at which the FiM to SPM transition occurs, appears to be ≈15 nm.

To affirm these findings, three sets of IONSs, each with a similar size ≈175, 230, and 380 nm, but differing in crystallite sizes,

ADVANCED
SCIENCE NEWS

www.advancedsciencenews.com

NANO · MICRO
small

www.small-journal.com
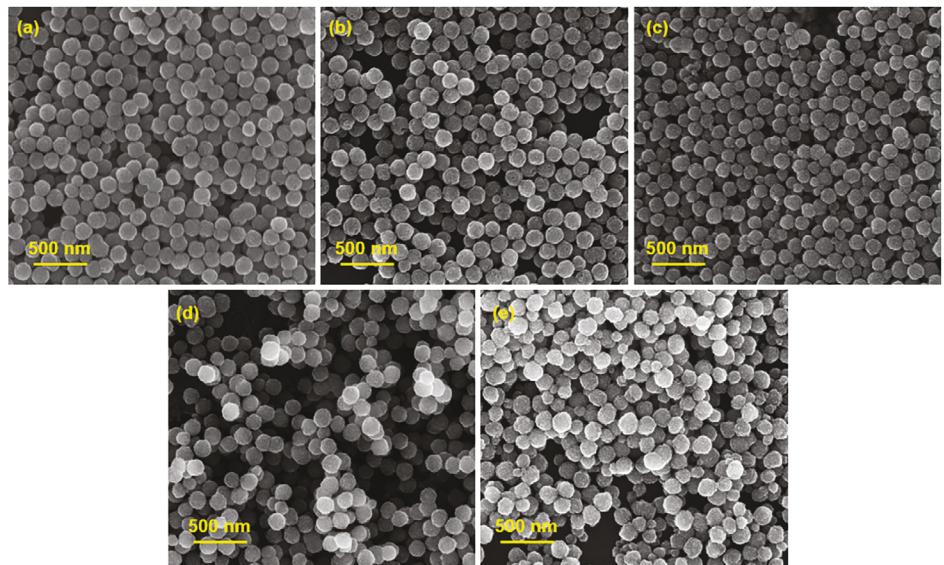
Figure 6. SEM images at 100 kX magnification of IONSs with similar average sizes: a) 157 ± 8 (cs 37 nm), b) 160 ± 10 (cs 26 nm), c) 159 ± 14 (cs 19 nm), d) 159 ± 11 (cs 12 nm), and (e) 159 ± 21 (cs 10 nm).

were synthesized and characterized to check the effects of crystallinity on the magnetic (FiM vs SPM) behaviors. **Figure 7** contrasts the SEM images of these samples, with a1, b1, and c1 for the highly crystalline FiM NPs (crystalline size, 26 to 34 nm), and a2, b2, c2 for the SPM NPs (crystallite size, 10 to 15 nm). As expected, the samples presented in Figure 7 (a1, b1, c1) display obvious magnetic hysteresis (Figure S8a, Supporting Information), signalizing the FiM characteristic. The samples presented in Figure 7 (a2, b2, c2) show no magnetic hysteresis (Figure S8b, Supporting Information), confirming their SPM nature at room temperature. These findings once again underscore the important role of crystallite size in controlling the nano-magnetism in magnetic nanoparticle systems.

The magnetization versus temperature measurements (M-T curves) under zero-field-cooled/field-cooled (ZFC/FC) protocol with small magnetic fields of 20 Oe were used to observe the Verwey transition (VT).[52] This VT transition is often used to confirm the existence of pure Fe_3O_4 phase and highly crystalline nature of magnetite samples.[17,52,53] Interestingly, as shown in Figure S9 (Supporting Information), the SPM sample with small crystallite size of ≈12 nm shows a discernable VT feature at ≈120–130 K in the ZFC curve. In the FC curve, there is also a slight drop in magnetization within this temperature range, indicating a good match with the VT transition observed in the ZFC. VT is usually easier to observe with single-crystalline samples.[52] For the polycrystalline IONSs in our work, the observation of VT in a sample with small crystallite size indicates the predominant magnetite phase of the samples and their high crystallinity.

2.4. Superparamagnetic Properties of Size-Tunable Polycrystalline IONSs

While it is not possible to achieve the SPM behavior in conventionally synthesized IONSs with large particle sizes (> 50 nm), our findings, as reported above, demonstrate this possibility in the presently studied polycrystalline IONSs. Indeed, we show in **Table 7** that IONSs with crystallite sizes < 15 nm (the critical SPM-size) exhibit the SPM behavior, even though their average particle size varies from ≈160 to 380 nm. The key to maintaining the SPM while tuning the size of NPs relies on the control of crystallite size ≤ 15 nm. The crystallite size of 15 nm is in the single-domain SPM region. Therefore, the SPM characteristic of the large polycrystalline IONSs in the size range of a few hundred nanometers can be understood as the collective SPM behaviors of their primary crystals, whose magnetic interactions within a polycrystalline particle are less significant.

Despite some works reporting the SPM behavior of large IONSs, a clear understanding of the temperature-dependent magnetization associated with the SPM to FiM transition has not been established.[32,36] Therefore, we conducted

Table 6. Magnetic properties of IONSs nanospheres with same size but different crystallite sizes.

Avg. Size [nm]	Crystallite Size [nm]	M_S [emu g^{-1}]	H_C [Oe]	M_r [emu g^{-1}]
157 ± 8	37	78	71	12
160 ± 10	26	75	62	9
159 ± 14	19	64	33	5
159 ± 11	12	63	≈0	≈0
159 ± 21	10	56	≈0	≈0
175 ± 13	34	79	77	10
175 ± 11	15	63	≈0	≈0
220 ± 10	26	73	41	5
234 ± 15	12	61	≈0	≈0
393 ± 27	24	67	16	3
375 ± 37	10	57	≈0	≈0

Data collected from VSM (presented in Figures S7 and S8, Supporting Information). Samples have SPM properties with no hysteresis loop and negligible values of M_r and H_C ($M_r = H_C = 0$).
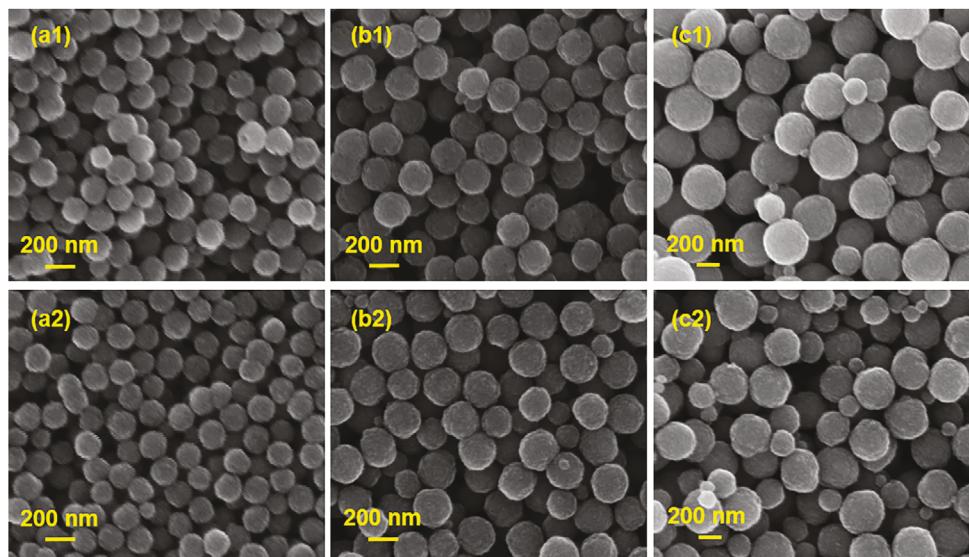
Figure 7. SEM images of IONSs with similar average size but having different crystallite sizes: a1) 175 ± 13 (cs 34 nm), a2) 175 ± 11 (cs 15), b1) 220 ± 10 (cs 26), b2) 235 ± 15 (cs 12), c1) 393 ± 27 (cs 24), c2) 375 ± 37 nm (cs 10 nm). Magnification 100 kX (a1, a2, b1, b2) and 60 kX (c1,c2).

magnetization versus temperature (M-T) measurements under zero-field-cooled/field-cooled (ZFC/FC) protocol for the SPM IONSs, which are displayed in Figure S10 (Supporting Information). Under an applied field of 500 Oe, a large separation between the ZFC and FC magnetization curves is observed for all samples investigated. All the samples show a broadened feature of ZFC M-T over a measured temperature range of 2–400 K, with the maxima value of ZFC below 300 K. The broadened feature of a ZFC M-T curve has been attributed to the presence of particle size distribution and inter-particle interactions.[54–58] In our case, clustering of primary nanocrystals forms a large particle; each particle can be considered as a multi-spin nanoclusters system. There thus exist multiple magnetic interactions in each sample, including intra- and inter-particle interactions between nanocrystals within a particle, and interactions among the particles. Effects of size distribution, including size distribution for nanocrystals that form a particle and for all particles within a sample, could also be considerable. For example, samples have similar standard deviation of about 10% of the mean value, such as large-size particles 200 ± 20 nm or small-size particles 20 ± 2 nm. Therefore, the broadening feature of the ZFC M-T curves observed for our samples (Figure S10, Supporting Information)

can be attributed to the size distribution of crystals and particles, as well as multiple magnetic interactions occurring within each particle and among particles.

The SPM behavior of large-sized magnetic particles is interesting and rarely reported. As discussed above, the nature of magnetic interactions, involving both intra- and inter-particle interactions, creates a more complicated system than that of common single-domain SPM nanoparticles with small sizes (< 25 nm). Figure S11 (Supporting Information) provides more details of the SPM properties in a large-sized sample, showing common SPM behavior observed in other SPM nanoparticles.[59–62] The hysteresis loop is observed at low temperatures below the blocking temperature, as shown in Figure S11a (Supporting Information). The broadening feature, which arises from the size distribution of primary crystals and particle sizes,[54–58] is consistently observed in the M-T curves at various applied fields (see Figures S10d and S11b–d, Supporting Information). At high fields, the VT transition might be suppressed due to the predominance of magnetic interactions. When increasing the applied field in the M-T measurements, the separation between the ZFC and FC curves narrows and eventually overlaps. The maximum magnetization region of the ZFC curve, commonly assumed to be the blocking temperature, shifts to a lower temperature as the applied field increases.[60–62] These features are commonly observed in other systems of SPM nanoparticles.[60–62] It is worth noting that due to the close interactions of nanocrystals in polycrystalline structures, a large magnetic field is needed to observe the blocking temperature feature in the ZFC curves.

Table 7. IONSs with SPM properties in a wide range of size from 160 to 380 nm.

Avg. Size [nm]	Crystallite Size [nm]	M_S [emu g^{-1}]	Magnetic Behaviors
159 ± 21	10	56	SPM
159 ± 11	12	63	SPM
175 ± 11	15	63	SPM
234 ± 15	12	61	SPM
271 ± 31	10	59	SPM
375 ± 37	10	57	SPM

2.5. Demonstrations for the Scale-Up Synthesis of Polycrystalline IONSs

To demonstrate the capability of method in scaling up, demonstrations with double scale-up produced highly uniform IONSs with tunable size and crystallite size were presented in **Figure 8**.
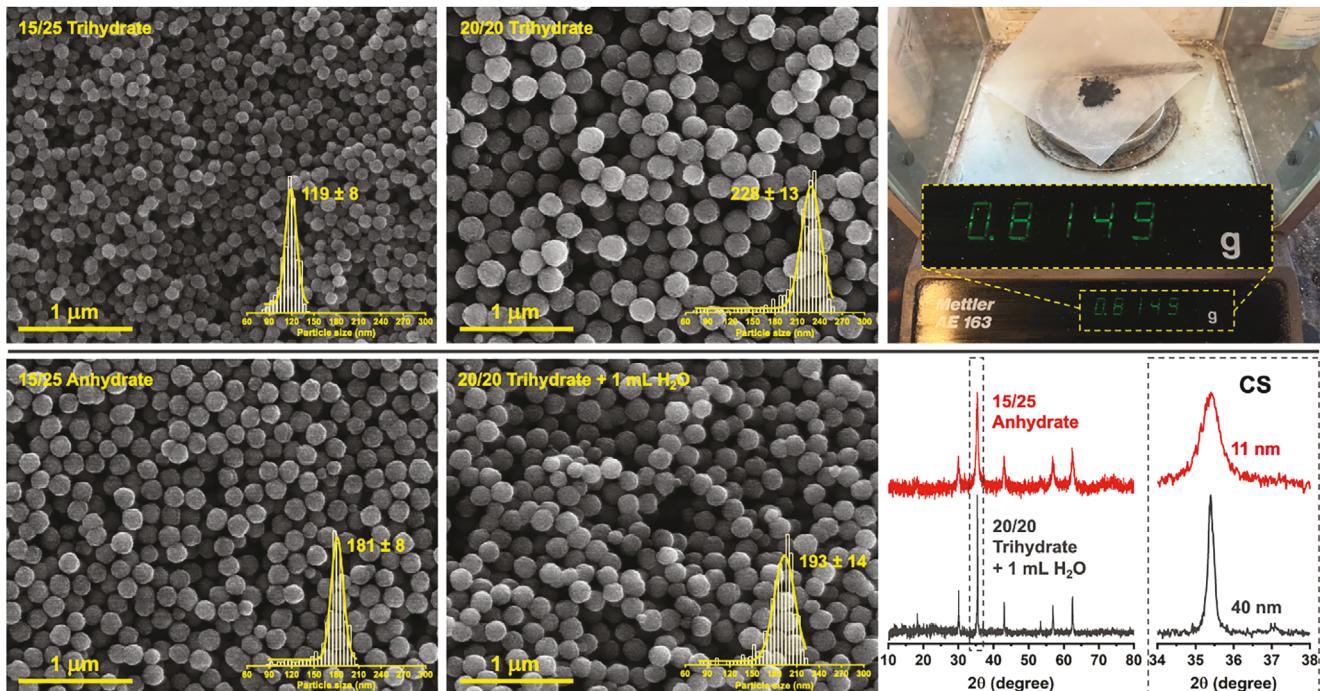
Figure 8. Scale up twice to synthesize iron oxide nanoparticles with tunable sizes and crystallite sizes.

The synthesis conditions and results are presented in Table S2 (Supporting Information). The synthesis at double scale was able to produce more than 0.8 g of high-quality IONSs. The first two conditions utilized sodium acetate trihydrate with solvent ratios of 15/25 mL and 20/20 mL EG/DEG perfectly replicate the result from the original scale reaction. Two samples with the size ≈180 to 190 nm and crystallite sizes of 11 and 40 nm were synthesized to demonstrate the capability of tuning the crystallinity. The phase composition of IONSs synthesized under scale-up conditions were characterized by Raman spectroscopy (see Figure S12, Supporting Information). Highly crystalline samples synthesized with NaAc·3H$_2$O additive exhibit a pure Fe$_3$O$_4$ phase.[44–46] The composition of the sample synthesized with an anhydrous NaAc additive, featuring small crystallite size of ≈11 nm, is a mixture of Fe$_3$O$_4$ and γ-Fe$_2$O$_3$ phases.[44–46] These results correspond well with those obtained at the original smaller reaction scale. The impact of chemical additives on particle structure and composition will be discussed in detail in Section 2.6. The success of scaling up the reaction was achieved thanks to the effectiveness and simplicity of the method. By following the same strategy in utilizing solvent compositions, adjusting the amount of water, using different amounts of additives, and controlling experimental parameters (ramping rate, stirring speed) as described in this work, we envision that producing large-scale uniform IONSs with tunable size and crystallite size can be achieved without any forceable challenges. It is worth noting that, compared to previous works discussed in Table 1, our method is significant not only in controlling the crystallinity and size of nanoparticles for widely and finely-tuning their magnetic properties, but also in producing IONPs with narrow size distributions and uniform spherical morphologies. Moreover, the ability to scale up while maintaining uniform morphologies is highly crucial. In-

terestingly, all of these capabilities in producing IONPs were achieved by simply adjusting the appropriate amount of chemical additives and using a versatile pressure vessel as the reaction container.

2.6. Proposed Mechanism of Growth of Polycrystalline Iron Oxide Nanoparticles

In this section, we discuss the proposed growth mechanism of NPs with the aim of providing guidance for optimizing the synthesis conditions to obtain iron oxide nanospheres (IONSs) with desired structures and properties. **Scheme 2** illustrates the process of IONSs formation. Generally, the rate of nucleation and the growth process primarily influence the size of the primary crystals (crystallite size), while the rate at which the primary crystals agglomerate affects the overall size of the particles. Fe^{3+} ions from FeCl$_3$ precursors initially precipitate as Fe(OH)$_3$ or FeOOH intermediates. Subsequently, the partial reduction of Fe^{3+} within Fe(OH)$_3$/FeOOH converts Fe^{3+} to Fe^{2+}, followed by dehydration, ultimately resulting in the formation of the Fe$_3$O$_4$ phase. Ethylene glycol (EG) and diethylene glycol (DEG) also play crucial roles as reducing agents, possibly converting into aldehydes or carboxylic acids.[7,24,63] We will now delve into a detailed discussion of the effects of each chemical component in the synthesis process.

The effects of additives (NaAc, H$_2$O, Na-acrylate) on phase compositions were studied by XPS, as presented in Figure S13 (Supporting Information). Three samples synthesized using anhydrous NaAc or with the addition of sodium acrylate, were subjected to analysis. High-resolution XPS Fe 2p spectra revealed that the sample synthesized with anhydrous NaAc exhibited a

$$(1) \quad CH_3COO^- + H_2O \rightleftharpoons CH_3COOH + OH^-$$

$$(2) \quad Fe^{3+} + 3\ OH^- \rightarrow Fe(OH)_3$$

$$(3) \quad Fe(OH)_3 \rightarrow FeOOH + H_2O$$

$$(4) \quad FeOOH + H_2O + e^- \rightarrow Fe(OH)_2 + OH^-$$

$$(5) \quad Fe(OH)_2 + 2\ FeOOH \rightarrow Fe_3O_4 + 2\ H_2O$$

$$(6) \quad Fe^{3+} + 6\ H_2O \rightarrow [\ Fe(H_2O)_6\ ]^{3+}$$
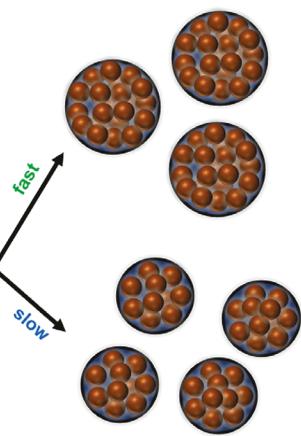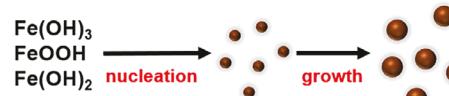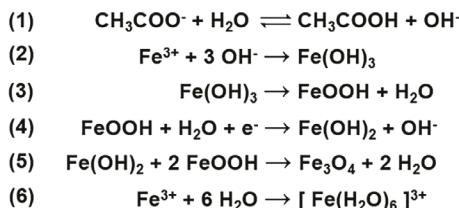
Scheme 2. Proposed mechanism for growing polycrystalline IONSs.

satellite peak at 718.7 eV, indicating the formation of γ-Fe$_2$O$_3$ phase.[41] Peaks at 724.1 and 710.3 eV were assigned to Fe 2p$_{3/2}$ and Fe 2p$_{1/2}$, respectively. We also observed a more brown or deep red-brown color of those samples synthesized with anhydrous NaAc, which suggested the presence of maghemite phase.[43] XPS spectra consistently displayed peaks at around 724.4 and 710.8 eV for samples synthesized with sodium acrylate additives, without observation of obvious satellite peaks in the 718 eV region. Therefore, the use of Na-acrylate additives did not appear to influence the compositions. However, the use of anhydrous sodium acetate led to the formation of the maghemite phase. Despite the fact the co-existence of magnetite (Fe$_3$O$_4$) and maghemite (γ-Fe$_2$O$_3$) is commonly observed, the existence of maghemite phase is a contributing factor that lowers the M$_S$ values.[64] In general, the broadening feature of peaks at $\approx$710 and 724 eV observed in all samples displayed the co-existence of Fe^{2+} and Fe^{3+} in samples, indicating the existence of a dominant Fe$_3$O$_4$ phase.

Water is the most critical factor in this mechanism. While an increase in the amount of water consistently led to a reduction in particle size, the crystallite size initially increased to an optimal level and subsequently decreased with further additions of water.[24] An appropriate quantity of water effectively promoted reactions (1), (2), and (4), thereby enhancing the rate of nucleation and the growth process, resulting in the formation of larger primary crystals. However, an excess of H$_2$O could induce the formation of complexes in reaction (6) and cause a dilution of the solvent system. This dilution, in turn, diminished the reductive capability of the solvent system (EG & DEG), thus slowing down the nucleation and growth process and resulting in a smaller crystallite size. Furthermore, H$_2$O played a crucial role in reaction (4), facilitating the partial reduction of Fe^{3+} to Fe^{2+} for the formation of the magnetite phase (Fe$_3$O$_4$). Therefore, the formation of the maghemite phase (γ-Fe$_2$O$_3$) when using anhydrous sodium acetate can be reasonably understood.

The size of particles is primarily influenced by the rate of the agglomeration process. Nanocrystals grow until they reach a certain size range where the monomer concentration is no longer sufficient to support further growth. At this point, the nanocrystals tend to agglomerate to reduce their surface energy. The rate of agglomeration is mainly affected by the polarity and viscosity of the solvent system, which are jointly influenced by EG, DEG, and H$_2$O. Bulky molecules with high boiling points, such as DEG, effectively slow the process, resulting in the formation of smaller particles. Similarly, a higher content of H$_2$O typically dilutes the solution, retarding the agglomeration process and leading to the formation of smaller particles. Moreover, water molecules exhibit a greater affinity for iron cations at the surface compared to EG, DEG, and PEG molecules, owing to their higher polarity and smaller molecular size. Consequently, a relatively small change in the amount of water, on the order of a few hundred µL, can lead to a more significant alteration in particle size compared to changes in the amounts of EG and DEG (Table S1, Supporting Information).

Sodium acetate serves as both an alkalinity controller and electrostatic stabilizer for the primary crystals. The presence of sodium acetate is essential for the formation of nanocrystals, primarily owing to its capacity to release OH$^-$ ions, which facilitate the precipitation of Fe(OH)$_3$. In contrast, sodium acrylate contributes less to the system's alkalinity due to the relatively small quantity used (100 to 200 mg). Additionally, the acidity of acrylic acid is higher than that of acetic acid, resulting in the conjugated sodium salt being less basic. Consequently, the limited amount of sodium acrylate employed does not significantly impact the size of NPs. Furthermore, sodium acrylate can undergo polymerization to form poly(acrylate) surfactants, potentially providing greater steric hindrance for primary crystals. However, this could have a detrimental effect, leading to a broader size distribution. Nevertheless, the presence of the double bond (H$_2$C=CH−COO(−)) in sodium acrylate may not impede the efficiency of electron transfer for reducing Fe^{3+} to Fe^{2+}. Therefore, the phase composition of the particles is unlikely to be affected. Diethylene glycol (DEG), apart from its role as a solvent and reducing agent, also acts as a surfactant due to structural similarities with polyethylene glycol (PEG). Thus, considering DEG as a capping agent explains the smaller particle size when a higher ratio of DEG composition is used. Considering all these complementary factors, we postulate that a balance among three components: EG, DEG, and H$_2$O is crucial to maintaining the optimal conditions for forming larger primary crystals, thereby enhancing the crystallinity of the NPs.

3. Conclusion

Synthesizing IONSs with tunable sizes and degree of crystallinity over a broad range has been successfully achieved through a comprehensive synthetic approach. This approach involves the judicious use of various additives (NaAc·3H$_2$O, H$_2$O, NaAc anhydrous, and Na-acrylate), precise manipulation of solvent compositions (EG & DEG mixture), and meticulous adjustments to stirring speed and heating rates in the solvothermal synthesis process. Remarkably, this endeavor has resulted in the production of highly crystalline iron oxide nanospheres, accompanied by a significant enhancement in FiM properties. Notably, this advancement has effectively narrowed the gap in FiM properties between spherical and cubic geometries. Furthermore, the ability to finely control the crystallinity of these IONSs across a wide range (from 10 to 37 nm) has endowed us with a versatile tool for tailoring the magnetic properties of IONSs. While both size and crystallinity influence the magnetic properties of IONSs, it is apparent that crystallinity assumes a more dominant role. This research offers a strategic methodology for synthesizing IONPs with desired magnetic properties by finely tuning their sizes and crystallite sizes. This versatile approach holds promise for a myriad of applications, which can be broadly categorized into three distinct types:

1) For applications requiring robust FiM properties, such as electronic devices, magnetic recording, and sensing, the utilization of large-sized highly crystalline IONPs with augmented FiM properties is particularly promising.

2) In the domains of biomedicine, biosensing, and drug delivery, large-sized SPM IONSs exhibit considerable potential, given their enhanced magnetism within the SPM regime.

3) Last, for applications requiring a moderate level of magnetism, such as magnetic separation or recoverable catalysts, the presented methodology represents a suitable tool for customizing magnetism to align with specific application requirements.

On-going works investigating insights into nano-magnetism and discovering biomedical applications of this polycrystalline nanoparticle system have been conducted. For the future perspectives, determining the primary crystal size (crystallite size) at which the transition from SPM to FiM behaviors occurs, as well as insights into the magnetic behaviors of large SPM IONSs, including their nano-magnetic characteristics and interparticle/crystal interactions, poses intriguing fundamental questions meriting further investigation.

4. Experimental Section

Materials: Iron(III) chloride hexahydrate (97%, Alfa Aesar) was used as precursor for synthesis of iron oxide nanospheres. Ethylene glycol (99%, Sigma–Aldrich) and Diethylene glycol (99%, ACROS Organics) were used as solvents. Sodium acetate (99%, anhydrous) was purchased from ACROS Organic and sodium acetate trihydrate (99%) was purchased from Fisher. Sodium acrylate (97%) was purchased from Sigma–Aldrich. Surfactant polyethylene glycol-400 was purchased from Olin Mathieson Chemical Corporation. Deionized water with resistance of 18 MΩ-cm (Academic Milli-Q Water System, Millipore Corporation). Pressure vessel used for synthesis of spherical IONSs was used with volume of 65 mL from

ChemGlass. For synthesis of Fe$_3$O$_4$ nanocubes, iron(III) acetylacetonate (99.9%), oleic acid (90%), and benzyl ether (98%), and 1-octadecene (90%) were all purchased from Sigma–Aldrich. Sodium oleate (97%) and 1-tetradecene (97%) were purchased from TCI. All chemicals were used for synthesis without any further purification.

Synthesis of Highly Crystalline Iron Oxide Nanospheres: A synthetic method for fabricating highly crystalline Fe$_3$O$_4$ nanospheres was developed based on reported solvothermal methods with modifications.[23,32,35] **Scheme 3** illustrates the procedure for synthesizing highly crystalline Fe$_3$O$_4$ nanospheres. Pressure vessels used for the synthesis of iron oxide nanospheres were cleaned in an aqua regia solution (3:1 HCl:HNO$_3$) and then dried overnight at 60 °C. Initially, a 40 mL mixture of a binary solvent system containing ethylene glycol (EG) and diethylene glycol (DEG) was prepared. To produce NPs with different sizes (average diameters), various ratios of the bi-solvent system EG/DEG (mL) were used: 10/30, 15/25, 20/20, and 30/10, resulting in nanospheres with average diameters of ≈50, 120, 220, and 390 nm, respectively. The process involved charging 1.35 g of FeCl$_3$·6H$_2$O into a pressure vessel with 20 mL of the solvent mixture and stirring for 15 min to dissolve the chemicals. Subsequently, 3.6 g of NaAc·3H$_2$O was added to the remaining half of the solvent mixture, and vigorous stirring continued for 30 min to form a homogeneous mixture. An aliquot of 1200 µL PEG(400) was then injected into the mixture, followed by heating it to 188 °C. Only under the synthetic condition using 10/30 EG/DEG mL was 1 mL of PEG(400) surfactant employed. The Teflon cap of the pressure vessel was securely screwed on, and a safety shield was used to cover the surroundings throughout the reaction. The ramping rate was maintained at ≈4.8 °C min^{-1}, and the reaction time was set to 5 h under vigorous stirring at least 540 rpm. The resulting product, which had a black color, was allowed to cool naturally to room temperature and was washed three times with ethanol, followed by magnetic separation. During each washing cycle, the IONPs in ethanol were sonicated for 15 min. In addition to solvent compositions, it was observed that stirring speed and ramping rate were two factors affecting the size of the NPs, as well as the homogeneity of their spherical morphology. By increasing the stirring speed by 20%, the conditions for synthesizing IONSs with an average size of 120 and 220 nm were adjusted to yield average sizes of 140 and 255 nm, respectively. Conversely, by increasing the ramp rate, the synthesis conditions could be altered to reduce the average size of the NPs. For instance, conditions to prepare NPs with a size of 120 nm (ramping rate ≈4.8 °C min^{-1}) were adjusted to produce IONSs with an average size of 89 nm by using a ramping rate of 11 °C min^{-1}. Therefore, the combination of stirring speed adjustments, ramp rates, and variations in solvent mixtures (EG & DEG) allowed for the production of IONSs with desired average sizes. Overall, this synthetic procedure efficiently yielded spherical NPs with homogeneous, spherical-like morphology, characterized by large crystallite sizes (ranging from 24 to 37 nm) and a uniform size distribution. Among different solvent compositions, a 15/25 (mL) EG/DEG ratio produced IONSs with the best crystalline structure and an average crystallite size of ≈34 to 37 nm was noted.

Additionally, the amount of water contained in trihydrate sodium acetate plays an important role in controlling the average size of NPs and their crystallinity was noticed. Instead of using 3.6 g of NaAc·3H$_2$O (which contains 2.17 g of NaAc and 1.43 mL of water), similar results (particle size and crystallite size) were achieved by using a combination of 2.17 g of NaAc (anhydrous chemical) and 1.43 mL of deionized water. Varying the amount of water can be used to change the size of NPs. For example, by adding an extra 0.54 mL of water, the synthetic conditions for preparing 220-nm nanospheres yielded Fe$_3$O$_4$ NPs with an average size of 175 nm and the crystallite size of 34 nm. Similarly, adding 0.54 mL of DI water to the synthetic conditions for a target size of 120 nm resulted in NPs with a size of 93 nm and a crystallite size of 34 nm. Therefore, adding water could be used to fabricate IONSs with different sizes and crystallite sizes. Experiments involving the addition of different amounts of water or the use of anhydrous NaAc are presented in Table S1 (Supporting Information).

Synthesis of Iron Oxides Nanospheres with Tunable Crystallite Sizes and Particle Sizes: To reduce the crystallite size of IONSs for shifting the magnetic properties toward weakly FiM or SPM properties, two approaches

**ADVANCED
SCIENCE NEWS**

www.advancedsciencenews.com

**NANO · MICRO
small**

www.small-journal.com
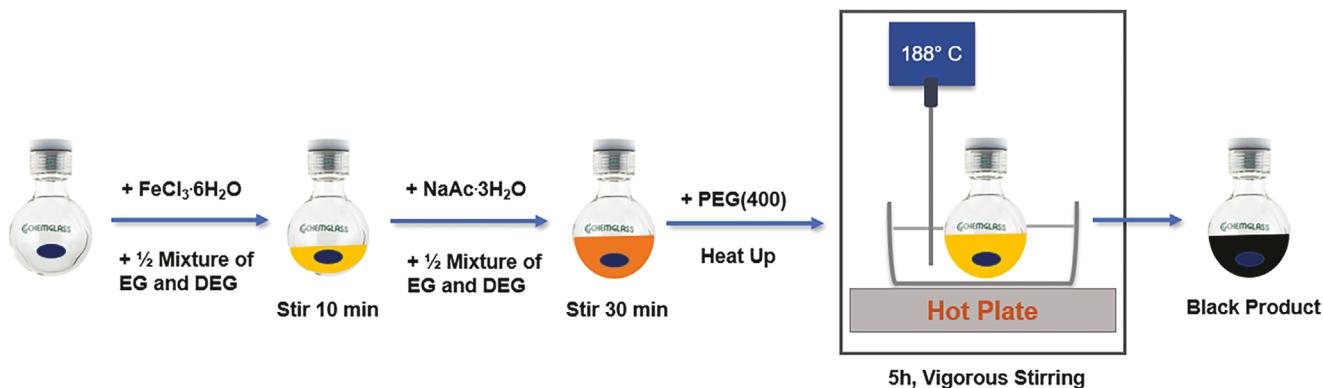
Scheme 3. Synthesis procedure for highly crystalline iron oxide nanospheres.

were employed: replacing NaAc·3H$_2$O with anhydrous NaAc or adding an extra amount of sodium acrylate (Na-acrylate) to decrease the average crystallite size. Generally, when 3.6 g of NaAc·3H$_2$O was replaced with 3.6 g of anhydrous NaAc while keeping other parameters constant, the average size of the NPs increased, but the crystallite size was significantly reduced to < 20 nm, as shown in Table S1 (Supporting Information). Similarly, to synthesize highly crystalline IONSs, anhydrous sodium acetate in combination was used with variations in the EG/DEG ratio and adjustments to stirring speed and ramping rate, resulting in various NP sizes with small crystallite sizes (< 20 nm). Different sets of IONSs were prepared with similar sizes ≈175, 230, and 380 nm but with varying crystallite sizes. Additionally, the addition of extra sodium acrylate, such as 100 or 200 mg, was shown to be effective in finely reducing the average crystallite size of IONSs while maintaining a consistent average size. For instance, when 100 or 200 mg of sodium acrylate was added to the synthetic conditions for IONSs (size 160 nm, crystallite size 26 nm), it was possible to produce IONSs with similar sizes while reducing the average crystallite sizes to 19 and 10 nm, respectively. However, the addition of sodium acrylate resulted in a broadening of the size distribution and deviations from spherical morphology in the synthesized NPs.

Importantly, following the trends in experimental parameters and the impact of chemical usage on tuning the NP structures (size and crystallite size) as described above is crucial references for guiding the synthesis of IONSs to a desired size and crystallinity.

Synthesis of Iron Oxide Nanocubes: The thermal decomposition of Fe(acac)$_3$ in benzyl ether solvent, supported by oleic acid surfactant, was used to prepare Fe$_3$O$_4$ nanocubes with a fast-ramping rate in a short refluxing time (30 min). The synthetic method was adapted from Hyeon's group with some modifications.[48] A two-neck round-bottom flask with a volume of 100 mL was used for all syntheses. The flask was cleaned with aqua regia (3:1 HCl:HNO$_3$), followed by a piranha solution (3:1 H$_2$SO$_4$:H$_2$O$_2$), and then dried in the oven overnight at 150 °C to completely remove all organic residues. Nanocube average sizes (edge length) ranging from 43 to 120 nm were synthesized by adjusting the stirring speed, concentration of precursors, and oleic acid surfactant.[37,48] Smaller Fe$_3$O$_4$ nanocubes (average size 23 ± 4 nm) were prepared by thermal decomposition with the addition of 4-biphenyl carboxylic acid. Growing large-size Fe$_3$O$_4$ nanocubes requires a stable medium over a longer period. Muro-Cruces reported using a tri-solvent system (benzyl ether, 1-octadecene, and 1-tetradecene) and two surfactants (sodium oleate and oleic acid) to offer better temperature stability during refluxing.[16] Consequently, nanocubes with a size of 184 nm were synthesized using a tri-solvent system and two surfactants (sodium oleate and oleic acid) with a refluxing time of 1 h. All synthetic conditions were conducted with a customized high-power 140 mW (J-KEM) heating mantle. The maximum heating power was used in all conditions with a heating rate of approximately ≈28 to 30 °C min^{-1}, and the refluxing time was maintained for 30 min. Nitrogen (N$_2$) degassing was performed for 2 h prior to the reaction, and minimum N$_2$ bubbling was maintained during the reaction.

Materials Characterization: Scanning electron microscope (SEM) LEO-1525 and FEI Dual Beam 235 Focused Ion Beam was used for imaging the NPs at operating voltage 15 kV. All samples were dissolved in ethanol and drop-casted on a clean surface of silicon wafer. Transmission electron microscope (TEM) JEOL JEM-2010 was used for imaging NPs and Selected Area Electron Diffraction of TEM was used to analyze the crystalline nature of the samples. The accelerating voltage of TEM was 200 kV. TEM grids 300-mesh holey carbon-coated copper grids were used. Powder X-ray Diffractometer (Smart Lab, Rigaku) using Cu Kα irradiations operated at 40 kV and 44 mA with a 0.01° step size was used for characterization of phase composition and to determine crystallinity. Samples were drop-casted on a clean glass slide surface for measurement. Full width at half maximum (FWHM) and θ of the most prominent peak of (311) planes at diffracted angle 2θ at 35.5° was used to calculate the average crystallite size, in accordance with other previous studies.[32,34–36] The average crystallite size was calculated by Debye–Scherrer formula, $D = \frac{K\lambda}{\beta \cos\theta}$ with K = 0.9 for spherical particles, λ = 0.15406 nm, β = FWHM (radians), and θ is the Bragg angle (radians). X-ray photoelectron spectroscopy (XPS) – PHI 5700 X-ray photoelectron spectrometer with a monochromatic Al Kα X-ray source was used to characterize the iron oxide powder samples. C 1s at binding energy 284.8 eV is used for calibration. The Raman scattering spectra of samples were measured with a Horiba JY T64000 triple spectrometer (laser beam 488 nm) coupled with an Olympus optical microscope. Dried powder samples with known mass (from 10 to 12 mg) were loaded in a capsule for measuring the magnetic properties, using a vibrating sample magnetometer (VSM) (LakeShore VSM 7300 Series with Controller LakeShore 735 and Gaussmeter LakeShore 450 and Software Version 3.8.0). Magnetization versus field (M-H) measurements were swept in the range of field ± 3kOe. Magnetic Property Measurement System (MPMS 3) by Quantum Design in DC mode was used to record the magnetization versus temperature (M-T) of the SPM samples. The M-T measurements were conducted following the typical zero-field-cooled/field-cooled (ZFC/FC) protocol at a selected magnetic field (from 20 to 2000 Oe).[39]

Supporting Information

Supporting Information is available from the Wiley Online Library or from the author.

Acknowledgements

Conflict of Interest

The authors declare no conflict of interest.

Data Availability Statement

The data that support the findings of this study are available from the corresponding author upon reasonable request.

[1] D. Lisjak, A. Mertelj, *Prog. Mater. Sci.* **2018**, *95*, 286.
[2] D. Bobo, K. J. Robinson, J. Islam, K. J. Thurecht, S. R. Corrie, *Pharm. Res.* **2016**, *33*, 2373.
[3] S. Liu, B. Yu, S. Wang, Y. Shen, H. Cong, *Adv. Colloid Interface Sci.* **2020**, *281*, 102165.
[4] S. Khizar, N. M. Ahmad, N. Zine, N. Jaffrezic-Renault, A. Errachid-el-salhi, A. Elaissari, *ACS Appl. Nano Mater.* **2021**, *4*, 4284.
[5] H. Gavilán, S. Kumar Avugadda, T. Fernández-Cabada, N. Soni, M. Cassani, B. T. Mai, R. Chantrell, T. Pellegrino, *Chem. Soc. Rev.* **2021**, *50*, 11614.
[6] Z. W. Tay, S. Savliwala, D. W. Hensley, K. L. B. Fung, C. Colson, B. D. Fellows, X. Zhou, Q. Huynh, Y. Lu, B. Zheng, P. Chandrasekharan, S. M. Rivera-Jimenez, C. M. Rinaldi-Ramos, S. M. Conolly, *Small Methods* **2021**, *5*, 2100796.
[7] J. Ji, Y. Huang, J. Yin, X. Zhao, X. Cheng, J. He, J. Wang, X. Li, J. Liu, *J. Phys. Chem. C* **2018**, *122*, 3628.
[8] G. C. Lavorato, R. Das, J. A. Masa, M.-H. Phan, H. Srikanth, *Nanoscale Adv.* **2021**, *3*, 867.
[9] X. Ge, J. Mohapatra, E. Silva, G. He, L. Gong, T. Lyu, R. P. Madhogaria, X. Zhao, Y. Cheng, A. M. Al-Enizi, A. Nafady, J. Tian, J. P. Liu, M.-H. Phan, F. Taraballi, R. I. Pettigrew, S. Ma, *Small* **2024**, *20*, 2306940.
[10] P. Q. Thong, L. T. Thu Huong, N. D. Tu, H. T. My Nhung, L. Khanh, D. H. Manh, P. H. Nam, N. X. Phuc, J. Alonso, J. Qiao, S. Sridhar, H. P. Thu, M. H. Phan, N. T. Kim Thanh, *Nanomedicine* **2022**, *17*, 1677.
[11] M. D. Nguyen, H.-V. Tran, S. Xu, T. R. Lee, *Appl. Sci.* **2021**, *11*, 11301.
[12] H.-V. Tran, N. M. Ngo, R. Medhi, P. Srinoi, T. Liu, S. Rittikulsittichai, T. R. Lee, *Materials* **2022**, *15*, 503.
[13] A. Feld, A. Weimer, A. Kornowski, N. Winckelmans, J.-P. Merkl, H. Kloust, R. Zierold, C. Schmidtke, T. Schotten, M. Riedner, S. Bals, H. Weller, *ACS Nano* **2019**, *13*, 152.
[14] L. Qiao, Z. Fu, J. Li, J. Ghosen, M. Zeng, J. Stebbins, P. N. Prasad, M. T. Swihart, *ACS Nano* **2017**, *11*, 6370.
[15] X. Tian, L. Ruan, S. Zhou, L. Wu, J. Cao, X. Qi, X. Zhang, S. Shen, *ACS Appl. Bio Mater.* **2022**, *5*, 1692.
[16] J. Muro-Cruces, A. G. Roca, A. López-Ortega, E. Fantechi, D. del-Pozo-Bueno, S. Estradé, F. Peiró, B. Sepúlveda, F. Pineider, C. Sangregorio, J. Nogues, *ACS Nano* **2019**, *13*, 7716.
[17] M.-H. Phan, J. Alonso, H. Khurshid, P. Lampen-Kelley, S. Chandra, K. Stojak Repa, Z. Nemati, R. Das, Ó. Iglesias, H. Srikanth, *Nanomaterials* **2016**, *6*, 221.
[18] K. M. Kirkpatrick, B. H. Zhou, P. C. Bunting, J. D. Rinehart, *Chem. Mater.* **2022**, *34*, 8043.
[19] M. Kampferbeck, L. R. Klauke, H. Weller, T. Vossmeyer, *Langmuir* **2021**, *37*, 9851.
[20] H. Gavilán, G. M. R. Rizzo, N. Silvestri, B. T. Mai, T. Pellegrino, *Nat. Protoc.* **2023**, *18*, 783.
[21] S. Sun, H. Zeng, *J. Am. Chem. Soc.* **2002**, *124*, 8204.
[22] J. Park, K. An, Y. Hwang, J.-G. Park, H.-J. Noh, J.-Y. Kim, J.-H. Park, N.-M. Hwang, T. Hyeon, *Nat. Mater.* **2004**, *3*, 891.
[23] H. Deng, X. Li, Q. Peng, X. Wang, J. Chen, Y. Li, *Angew. Chem., Int. Ed.* **2005**, *44*, 2782.
[24] Y. Liu, T. Cui, Y. Li, Y. Zhao, Y. Ye, W. Wu, G. Tong, *Mater. Chem. Phys.* **2016**, *173*, 152.
[25] T. Balakrishnan, M.-J. Lee, J. Dey, S.-M. Choi, *CrystEngComm* **2019**, *21*, 4063.
[26] P. K. Narnaware, C. Ravikumar, *J. Phys. Chem. C* **2020**, *124*, 25010.
[27] R. Chen, M. G. Christiansen, A. Sourakov, A. Mohr, Y. Matsumoto, S. Okada, A. Jasanoff, P. Anikeeva, *Nano Lett.* **2016**, *16*, 1345.
[28] M. Unni, A. M. Uhl, S. Savliwala, B. H. Savitzky, R. Dhavalikar, N. Garraud, D. P. Arnold, L. F. Kourkoutis, J. S. Andrew, C. Rinaldi, *ACS Nano* **2017**, *11*, 2284.
[29] A. N. Solodov, J. R. Shayimova, E. A. Burilova, D. V. Shurtakova, Y. I. Zhuravleva, M. A. Cherosov, Y. Tian, A. G. Kiiamov, R. R. Amirov, *J. Phys. Chem. C* **2021**, *125*, 20980.
[30] H. Chang, B. H. Kim, H. Y. Jeong, J. H. Moon, M. Park, K. Shin, S. I. Chae, J. Lee, T. Kang, B. K. Choi, J. Yang, M. S. Bootharaju, H. Song, S. H. An, K. M. Park, J. Y. Oh, H. Lee, M. S. Kim, J. Park, T. Hyeon, *J. Am. Chem. Soc.* **2019**, *141*, 7037.
[31] I. Castellanos-Rubio, O. Arriortua, D. Iglesias-Rojas, A. Barón, I. Rodrigo, L. Marcano, J. S. Garitaonandia, I. Orue, M. L. Fdez-Gubieda, M. Insausti, *Chem. Mater.* **2021**, *33*, 8693.
[32] S. Xuan, Y.-X. J. Wang, J. C. Yu, K. Cham-Fai Leung, *Chem. Mater.* **2009**, *21*, 5079.
[33] Y. Chen, J. Zhang, Z. Wang, Z. Zhou, *Appl. Sci.* **2019**, *9*, 5157.
[34] S. Xuan, F. Wang, Y.-X. J. Wang, J. C. Yu, K. Cham-Fai Leung, *J. Mater. Chem.* **2010**, *20*, 5086.
[35] Y.-T. Chen, R. Medhi, I. Nekrashevich, D. Litvinov, S. Xu, T. R. Lee, *Anal. Chem.* **2018**, *90*, 6749.
[36] J. Ge, Y. Hu, M. Biasini, W. P. Beyermann, Y. Yin, *Angew. Chem., Int. Ed.* **2007**, *46*, 4342.
[37] A. G. Kolhatkar, Y.-T. Chen, P. Chinwangso, I. Nekrashevich, G. C. Dannangoda, A. Singh, A. C. Jamison, O. Zenasni, I. A. Rusakova, K. S. Martirosyan, D. Litvinov, S. Xu, R. C. Willson, T. R. Lee, *ACS Omega* **2017**, *2*, 8010.
[38] W. E. M. Elsayed, F. S. Al-Hazmi, L. S. Memesh, L. M. Bronstein, *Colloids Surf. A Physicochem. Eng. Asp.* **2017**, *529*, 239.
[39] Z. Nemati, J. Alonso, I. Rodrigo, R. Das, E. Garaio, J. Á. García, I. Orue, M.-H. Phan, H. Srikanth, *J. Phys. Chem. C* **2018**, *122*, 2367.
[40] S. D. Shingte, A. H. Phakatkar, E. McKiernan, K. Nigoghossian, S. Ferguson, R. Shahbazian-Yassar, D. F. Brougham, *Chem. Mater.* **2022**, *34*, 10801.
[41] T. Yamashita, P. Hayes, *Appl. Surf. Sci.* **2008**, *254*, 2441.
[42] A. P. Grosvenor, B. A. Kobe, M. C. Biesinger, N. S. McIntyre, *Surf. Interface Anal.* **2004**, *36*, 1564.
[43] R. M. Cornell, U. Schwertmann, *The Iron Oxides: Structure, Properties, Reactions, Occurrences and Uses*, John Wiley & Sons, New Jersey, USA **2003**.
[44] I. Chamritski, G. Burns, *J. Phys. Chem. B* **2005**, *109*, 4965.
[45] M. Hanesch, *Geophys. J. Int.* **2009**, *177*, 941.

[46] R. Otero-Lorenzo, M. A. Ramos-Docampo, B. Rodríguez-González, M. Comesaña-Hermo, V. Salgueiriño, *Chem. Mater.* **2017**, *29*, 8729.

[47] Z. Nemati, R. Das, J. Alonso, E. Clements, M. H. Phan, H. Srikanth, *J. Electron. Mater.* **2017**, *46*, 3764.

[48] D. Kim, N. Lee, M. Park, B. H. Kim, K. An, T. Hyeon, *J. Am. Chem. Soc.* **2009**, *131*, 454.

[49] K. J. Klabunde, R. M. Richards, *Nanoscale Materials in Chemistry*, John Wiley & Sons, New Jersey, USA **2009**.

[50] Z. Xu, C. Shen, Y. Hou, H. Gao, S. Sun, *Chem. Mater.* **2009**, *21*, 1778.

[51] A.-H. Lu, E. L. Salabas, F. Schüth, *Angew. Chem., Int. Ed.* **2007**, *46*, 1222.

[52] R. Das, J. Alonso, Z. Nemati Porshokouh, V. Kalappattil, D. Torres, M.-H. Phan, E. Garaio, J. Á. García, J. L. Sanchez Llamazares, H. Srikanth, *J. Phys. Chem. C* **2016**, *120*, 10086.

[53] M. Bohra, N. Agarwal, V. Singh, *J. Nanomater.* **2019**, *2019*, 1.

[54] W. Xu, M. Ji, Y. Chen, H. Zheng, L. Wang, D.-L. Peng, *J. Phys. Chem. C* **2021**, *125*, 5880.

[55] R. K. Zheng, H. Gu, B. Xu, X. X. Zhang, *J. Phys.: Condens. Matter* **2006**, *18*, 5905.

[56] R. Sappey, E. Vincent, N. Hadacek, F. Chaput, J. P. Boilot, D. Zins, *Phys. Rev. B* **1997**, *56*, 14551.

[57] K. L. Livesey, S. Ruta, N. R. Anderson, D. Baldomir, R. W. Chantrell, D. Serantes, *Sci. Rep.* **2018**, *8*, 11166.

[58] N. A. Frey, M. H. Phan, H. Srikanth, S. Srinath, C. Wang, S. Sun, *J. Appl. Phys.* **2009**, *105*, 07B502.

[59] W. Wu, Z. Wu, T. Yu, C. Jiang, W.-S. Kim, *Sci. Technol. Adv. Mater.* **2015**, *16*, 023501.

[60] W. Wu, X. Xiao, S. Zhang, T. Peng, J. Zhou, F. Ren, C. Jiang, *Nanoscale Res. Lett.* **2010**, *5*, 1474.

[61] A. A. Krasikov, Y. V. Knyazev, D. A. Balaev, D. A. Velikanov, S. V. Stolyar, Y. L. Mikhlin, R. N. Yaroslavtsev, R. S. Iskhakov, *Physica B Condens. Matter* **2023**, *660*, 414901.

[62] Q. Chen, Z. J. Zhang, *Appl. Phys. Lett.* **1998**, *73*, 3156.

[63] Y. Wang, Y. Zheng, C. Z. Huang, Y. Xia, *J. Am. Chem. Soc.* **2013**, *135*, 1941.

[64] M. Colombo, S. Carregal-Romero, M. F. Casula, L. Gutiérrez, M. P. Morales, I. B. Böhm, J. T. Heverhagen, D. Prosperi, W. J. Parak, *Chem. Soc. Rev.* **2012**, *41*, 4306.